



University of HUDDERSFIELD

University of Huddersfield Repository

Dale, Matthew W. and Wedge, Christopher J.

Optically generated hyperpolarization for sensitivity enhancement in solution-state NMR spectroscopy

Original Citation

Dale, Matthew W. and Wedge, Christopher J. (2016) Optically generated hyperpolarization for sensitivity enhancement in solution-state NMR spectroscopy. *Chemical Communications*, 52 (90). pp. 13221-13224. ISSN 1359-7345

This version is available at <http://eprints.hud.ac.uk/id/eprint/30367/>

The University Repository is a digital collection of the research output of the University, available on Open Access. Copyright and Moral Rights for the items on this site are retained by the individual author and/or other copyright owners. Users may access full items free of charge; copies of full text items generally can be reproduced, displayed or performed and given to third parties in any format or medium for personal research or study, educational or not-for-profit purposes without prior permission or charge, provided:

- The authors, title and full bibliographic details is credited in any copy;
- A hyperlink and/or URL is included for the original metadata page; and
- The content is not changed in any way.

For more information, including our policy and submission procedure, please contact the Repository Team at: E.mailbox@hud.ac.uk.

<http://eprints.hud.ac.uk/>

Electronic Supplementary Information

Optically generated hyperpolarization for sensitivity enhancement in solution-state NMR spectroscopy

Matthew W. Dale and Christopher J. Wedge

Department of Physics, University of Warwick, Coventry, CV4 7AL UK

Email: chris.wedge@chch.oxon.org

Experimental details

Preparation of samples

2,2,6,6-tetramethylpiperidine 1-oxyl (TEMPO, 98 % purity) and rose bengal disodium salt (95 %), both purchased from Sigma Aldrich, were used without further purification and dissolved in either Milli-Q water, or a 1:4 mixture of Milli-Q water and deuterium oxide (Sigma, 99.9%). Nitrogen gas, sourced from liquid nitrogen boil-off, was bubbled through each sample in a gas tight syringe (SGE) for 10 minutes to remove dissolved oxygen before injection into a nitrogen purged flow system at a continuous rate using a calibrated syringe pump (Legato 110).

Flow system

To reduce the diffusion of oxygen into the solution during transfer to the probe, the flow system used concentric PTFE and PVC tubes. The inner PTFE tube (inner diameter (ID) 1/32") carried the solution, while the outer PVC tube enclosed the PTFE tube and was purged with room temperature dry nitrogen, sourced from liquid nitrogen boil-off. The purge entered the PVC tube through a T-section adjoining the syringe (Fig. S1a), and continued into the quartz sample cell (also with a two layer concentric construction) before exiting above the sample volume. An additional benefit of the purge is that it reduced heating of the sample during illumination.

The sample cell (Fig. S1b), centered in the RF coil, was comprised of a quartz tube of ID 1 mm and outer diameter (OD) 2 mm centered inside a second quartz tube of ID 3 mm for structural support. The height of the sample volume was 5 mm, with solution flowed to and from it through quartz tubes of ID 0.5 mm. The reduced diameter of flow tubes to and from the sample volume increased the proportion of illuminated solution in the sensitive region of the RF coil, which extended above and below the illuminated region. Solution exited by a PTFE tube through the top of the probe.

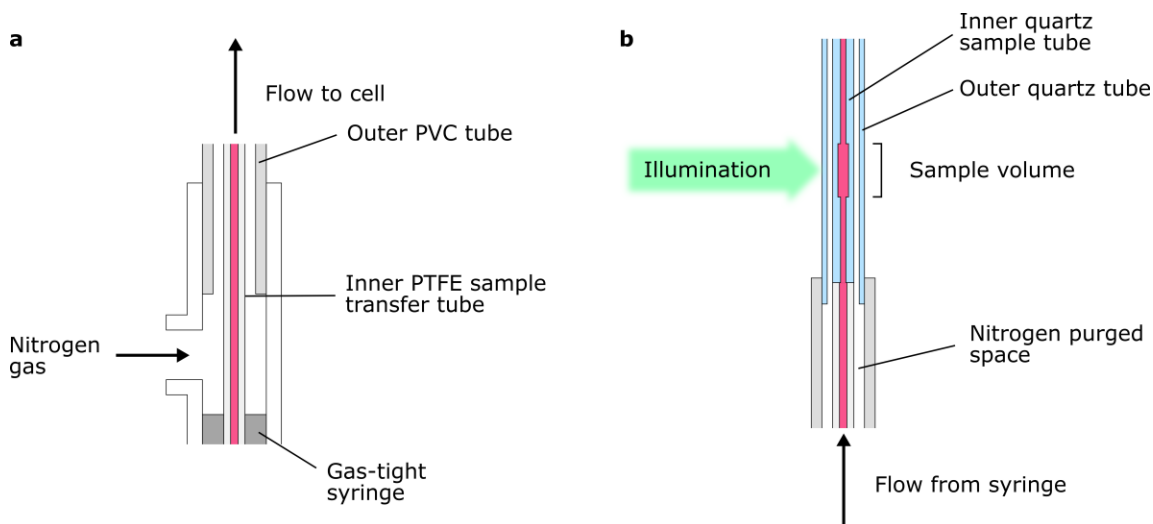


Fig. S1. Diagram of flow system used. (a) Nitrogen purge entered an outer tube adjacent to the syringe to prevent diffusion of oxygen into the solution. (b) The connection and construction of the sample cell. The sample tube was restricted above and below the illuminated volume to reduce the quantity of solution in the sensitive region of the RF coil which was not illuminated. An outer jacket was used from the syringe pump to the sample volume and the space between purged with nitrogen gas.

NMR system

NMR measurements were made with a Bruker Avance spectrometer. The external magnetic field was supplied by the electromagnet system of a Bruker E580 X/Q-band EPR spectrometer. For the NMR probe a Bruker X-band EPR ENDOR resonator was used (EN 4118X-MD4). The radiofrequency (RF) coil was tuned and matched to the NMR receiver with an external circuit. The magnetic field for all experiments was 0.342 T, corresponding to a ^1H NMR frequency of 14.6 MHz. No standard was used so the chemical shift scales given are unreferenced.

The homogeneous linewidth of an EPR transition is typically much broader than an NMR transition and so there are less stringent demands of magnet homogeneity; as such the magnets used for EPR spectroscopy are typically not shimmed. In this case the field homogeneity over the illuminated sample volume was approximately 1 ppm, however the field homogeneity of the whole NMR sensitive region, including the flow tubes, was approximately 5 ppm. This is the cause of the distorted lineshape of all NMR spectra shown.

Illumination

Illumination for optical generation of dynamic nuclear polarization (DNP) was by a laser diode (NLD521000G, Roithner LaserTechnik), outputting 1 W at 520 nm, of which 840 mW was incident on the resonator window (rated at 90% transmission). The focus of the laser was adjusted to fill the sample volume (Fig. S1b). Continuous illumination was used for all DNP experiments.

EPR measurements

Time-resolved electron paramagnetic resonance (EPR) measurements were made in a Bruker E580 X/Q-band EPR spectrometer as for NMR measurements. Pulsed illumination was with a Continuum Surelite I, frequency doubled Nd:YAG laser. The repetition rate of the laser was 20 Hz with a pulse width of approximately 5 ns and a pulse energy of 5 mJ at 532 nm used. The laser beam had a diameter of approximately 6 mm and filled the sample volume through the resonator window. The EPR signal was measured at a variable delay relative to the laser pulse, using a standard two pulse echo sequence ($90^\circ - \tau - 180^\circ - \tau - \text{echo}$) with four-step phase cycle.

Supplementary data

Absorption spectra

The absorption spectra of the rose bengal dye and TEMPO radical are shown in Fig. S2. At 520 nm, the laser is strongly absorbed by the rose bengal but weakly absorbed by the TEMPO. Although UV illumination has been used in previous investigations of radical-triplet pair spin polarization of xanthenes dyes,¹ it is more strongly absorbed by TEMPO than visible wavelengths so can lead to degradation of the radical. Illuminating in the 500 – 550 nm absorption band of rose bengal was found to be more effective at generating spin polarization, although owing to the higher extinction coefficient of the dye in this band concentrations must be reduced to maintain the same optical absorbance.

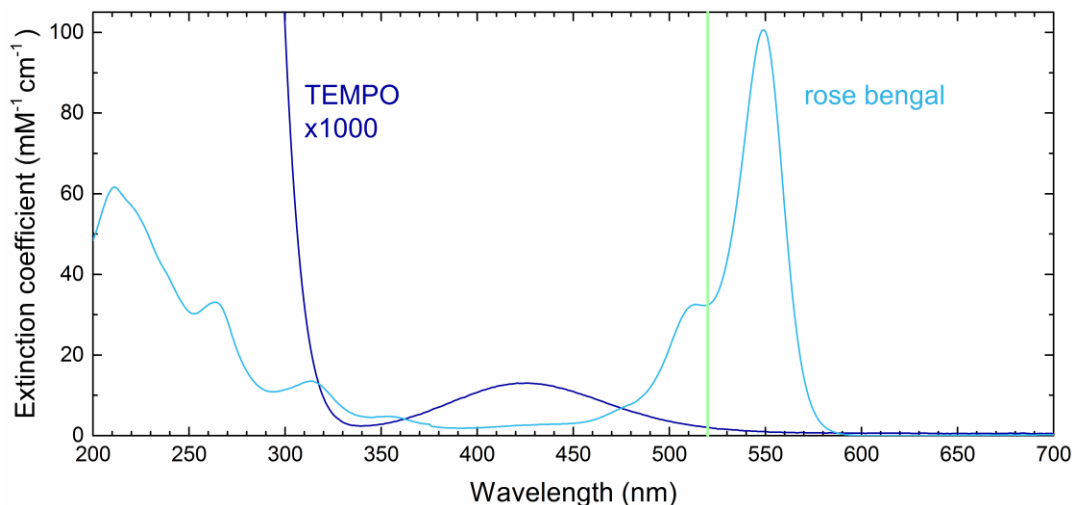


Fig. S2. Absorption spectra of TEMPO and rose bengal dye in aqueous solution. The TEMPO absorption has been multiplied by 1000 for comparison with the much more intense absorption of rose bengal. The wavelength of the excitation used for DNP experiments is indicated.

At 520 nm, the 0.2 mM rose bengal has an absorption coefficient of 6.5 cm^{-1} (Fig. S2). The sample tube was cylindrical with a diameter of 1 mm, giving transmission of approximately 22 % of the laser light normally incident on the tube centre. In adjusting the absorption coefficient a balance must be made between the light not being absorbed and failure of the light to penetrate the sample. An absorbance of around 1 for the path length used is expected to be a good compromise. A comparison of the spin polarized NMR signal is shown in Fig. S3 for several concentrations of rose bengal with 1.0 mM TEMPO. The 0.2 mM rose bengal solution was most effective.

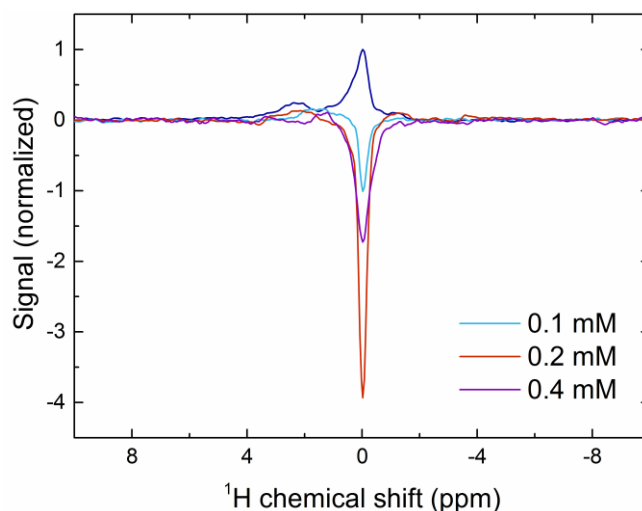


Fig. S3. ^1H NMR signal with 1 W illumination at 520 nm for solutions of 1 mM TEMPO and 0.1, 0.2 or 0.4 mM rose bengal in partially deuterated water (1:4 $\text{H}_2\text{O}/\text{D}_2\text{O}$). The dark signal (positive) is also shown for comparison.

Sample deoxygenation

Deoxygenation of the sample was found to be critical in creating nuclear polarization. Fig. S4 shows a comparison of the ^1H NMR spectra under illumination with and without the previously described deoxygenation procedure and purged flow system. The reduction of nuclear spin polarization in the presence of oxygen supports the interpretation that the polarization is generated by the radical-triplet pair mechanism. Molecular oxygen is a ground-state triplet which efficiently quenches excited triplet states through a spin allowed process, resulting in generation of singlet oxygen. Dissolved oxygen strongly quenches the triplet state of the dye, competing with triplet-radical quenching events and hence reduces electron, and therefore nuclear, spin polarization. Spin relaxation will also be accelerated by the presence of paramagnetic oxygen.

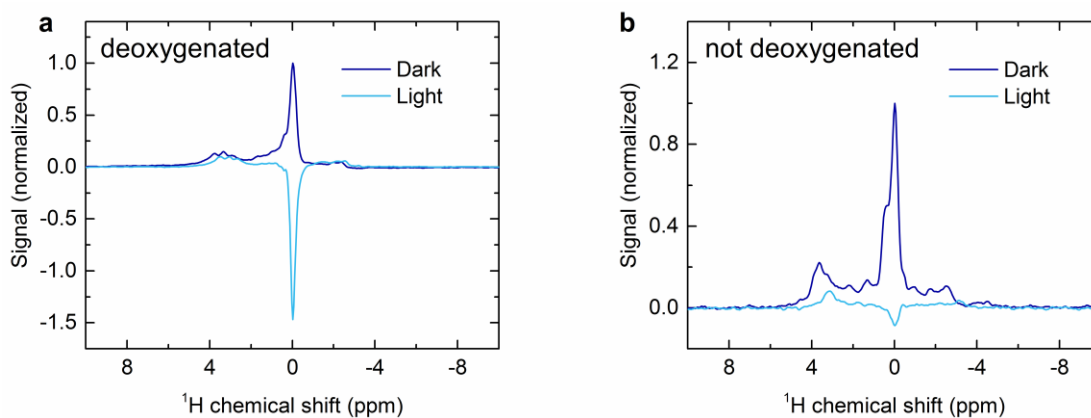


Fig. S4. ^1H NMR spectra of an aqueous solution of 0.2 mM rose bengal and 1 mM TEMPO, in the presence and absence of 520 nm illumination (1 W). Spectra were recorded (a) with and (b) without deoxygenation by nitrogen bubbling.

Sample flow rate

The sample flow rate was an important parameter for optimizing the signal enhancement. An example of the response of the enhancement to flow rate is shown in Fig. S5 where the optimum flow rate was $10 \mu\text{l min}^{-1}$. The change in the measured polarization with flow rate results from a combination of the build-up time for nuclear polarization and degradation of the dye. In the absence of illumination the NMR signal intensity was not affected by flow rates below $50 \mu\text{l min}^{-1}$. The optimum flow rate was also dependent on the radical concentration but was always found to be in the range $5 - 15 \mu\text{l min}^{-1}$.

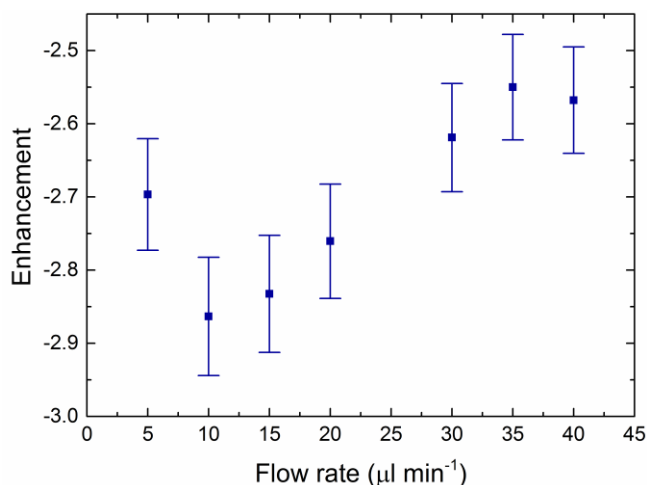


Fig. S5. Enhancement factor versus the sample flow rate for an aqueous solution of 0.2 mM rose bengal and 1 mM TEMPO. A reduction is seen in the enhancement at low flow rates due to bleaching of the dye, and at high flow rates as insufficient time is allowed for nuclear polarization build-up before the solution leaves the active region of the NMR coil.

Laser power dependence

NMR enhancement was found to increase with laser intensity, Fig. S6. Laser power dependence will arise from interplay between the concentration of triplets generated and rate of photodegradation, hence for none photostable dyes such as rose bengal will vary with sample flow rate. Laser intensity influences overall enhancement by changes in the saturation factor, which as we have shown is also dependent on radical concentration (Fig. 3b). Further studies into the effects of laser intensity and illumination time are ongoing using an upgraded laser source (532 nm Diode Pumped Solid State Laser, Roithner MGL-532).

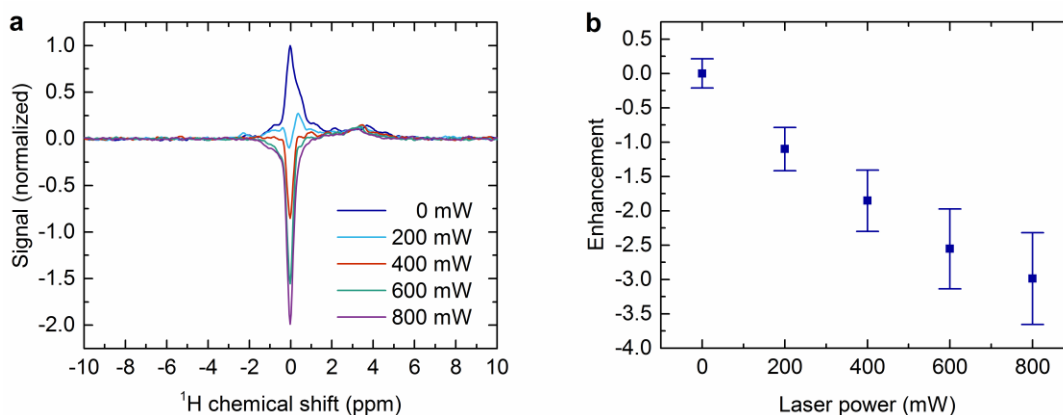


Fig. S6. Enhancement of ^1H NMR signal of water solvent. (a) ^1H NMR spectra of a solution of 0.2 mM rose bengal and 1.0 mM TEMPO in partially deuterated water (1:4 $\text{H}_2\text{O}/\text{D}_2\text{O}$), with laser illumination at 532 nm at various powers on resonator window as indicated. (b) The corresponding enhancement factor as a function of laser power. Sample flow rate $20 \mu\text{l min}^{-1}$.

Sample temperature

The continuous nitrogen gas flow around the sample acts to prevent any significant heating as a result of laser illumination. It is difficult to directly measure the sample temperature, but an estimate can be obtained through measurement of the spin lattice relaxation time T_{1n} of the water protons.²⁻³ Relaxation data measured using an inversion recovery sequence are shown in Fig. S7 as a function of illumination power. An increase from around 2.5 s to 3.2 s is observed for illumination at full power with gas cooling applied. While there is some variation in literature values for T_{1n} of bulk water making it difficult to obtain an absolute value, a change of this order of magnitude appears to correspond to an increase of less than 10 K, significantly less than might be expected for microwave heating in conventional Overhauser DNP without severed restriction of sample volume.⁴

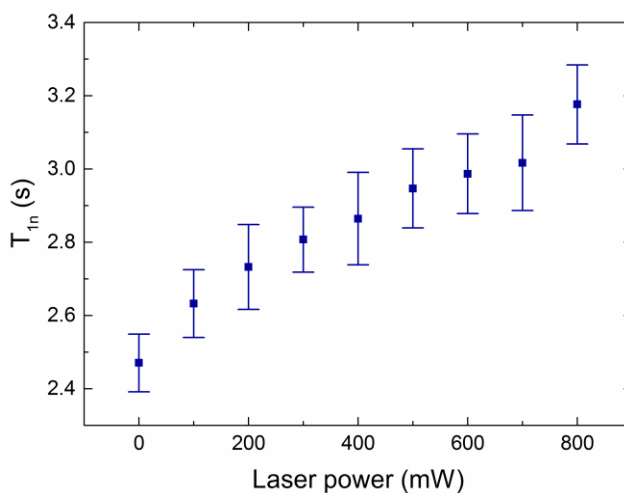


Fig. S7. ^1H spin-lattice relaxation time measured by inversion recovery as a function of 520 nm laser illumination power measured at resonator window. The aqueous sample contained 0.2 mM rose bengal without TEMPO radical, and the flow rate was $10 \mu\text{l min}^{-1}$. In all cases the sample was deoxygenated by nitrogen bubbling and a continuous nitrogen gas flow acted to cool the sample.

Data deposition

Data created during this research are openly available from the University of Warwick Research Archive Portal at <http://wrap.warwick.ac.uk/81788>

Energy level diagram

The energy levels of a radical triplet pair are shown schematically in Fig. S8. At large separations the spin states of the triplet ($|T_+\rangle$, $|T_0\rangle$, and $|T_-\rangle$) and radical ($|\alpha\rangle$, and $|\beta\rangle$) can be treated independently. As the separation is reduced due to an encounter in solution it is more appropriate to consider the overall spin states arising from the coupling of the triplet ($S_T = 1$) and radical ($S_R = 1/2$). The total spin takes values $S = S_T + S_R, S_T + S_R - 1, \dots, |S_T - S_R| = 3/2, 1/2$ hence quartet and doublet manifolds must be considered. These are separated by the radical triplet exchange energy which for a typical antiferromagnetic coupling leads to the quartet states being higher in energy. For further details, including the composition of the coupled states as linear combinations of the uncoupled states, the interested reader is referred to refs 5 – 7, and for a review of all chemically induced dynamic electron polarization mechanisms to ref. 8.

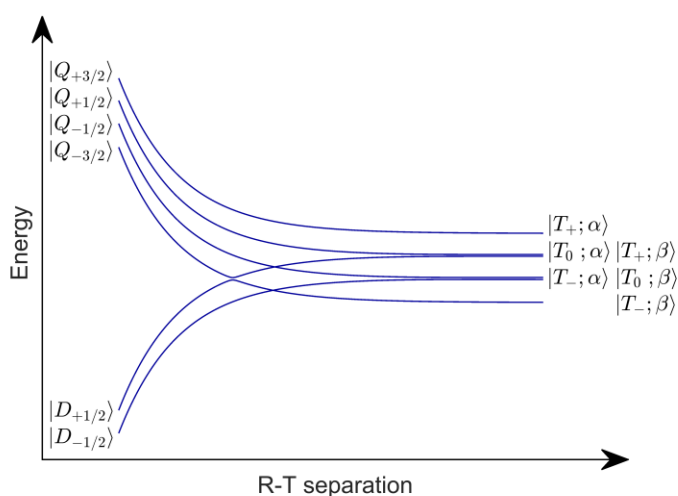


Fig. S8. Energy level diagram of a radical triplet pair. Modulation of the zero-field splitting of the triplet leads to an avoided crossing between $|D_{+1/2}\rangle$ and $|Q_{-3/2}\rangle$ which results in the radical gaining a non-Boltzmann spin polarization.

References

- (1) H. Takahashi, M. Iwama, N. Akai, K. Shibuya and A. Kawai, *Mol. Phys.* 2014, **112**(7), 1012–1020.
- (2) J.H. Simpson and H.Y. Carr, *Phys. Rev.* 1958, **111**(5), 1201–1202.
- (3) J.C. Hindman, A. Svirnickas and M. Wood, *J. Chem. Phys.* 1973, **59**(3), 1517–1522.
- (4) M.-T. Turke, I. Tkach, M. Reese, P. Hofer and M. Bennati, *Phys. Chem. Chem. Phys.*, 2010, **12**, 5893–5901.
- (5) C. Blättler, F. Jent and H. Paul, *Chem. Phys. Lett.* 1990, **166**(4), 375–380.
- (6) A. Kawai and K. Shibuya, *J. Photochem. Photobiol., C* 2006, **7**, 89–103.
- (7) A.I. Shushin, *J. Phys. Chem. A* 2014, **118**, 11355–11363.
- (8) M.D.E. Forbes, L.E. Jarocho, SY Sim and V.F. Tarasov, *Adv. Phys. Org. Chem.* 2013, **47**, 1–83.